nature photonics

SUPPLEMENTARY INFORMATION

DOI: 10.1038/NPHOTON.2016.107

Optical transduction and routing of microwave phonons in cavity-optomechanical circuits

Kejie Fang,[1,2] Matthew H. Matheny,[1,2] Xingsheng Luan,[1,2] and Oskar Painter[1,2,*]

[1] *Kavli Nanoscience Institute and Thomas J. Watson, Sr., Laboratory of Applied Physics, California Institute of Technology, Pasadena, California 91125, USA*

[2] *Institute for Quantum Information and Matter, California Institute of Technology, Pasadena, California 91125, USA*

(Dated: April 7, 2016)

I. DESIGN OF MECHANICAL CAVITY AND WAVEGUIDE COUPLING

In the optomechanical cavity-waveguide coupled devices, we can change the cavity-waveguide coupling (i.e. γ_e) on purpose. This is achieved by the design of a low-Q mechanical cavity mode and varying the number of mirror cells (Fig. S-1a). As shown in Fig. S-1b, the blue curves are the mechanical band structure of the mirror unit cell (blue rectangle in Fig. S-1a). We design the cavity such that the mechanical cavity frequency (red dashed line in Fig. S-1b) overlaps with the band of mirror unit cell, such that the mechanical cavity mode can tunnel through the mirror cells into waveguide. Meanwhile, the optical cavity frequency (red dashed line in Fig. S-1c) lies within the optical band gap of mirror unit cell, such that the optical cavity mode keeps high-Q. By varying the number of unit cells, we find the simulated radiation mechanical coupling rate into waveguide ($\gamma_e/2\pi$) oscillates between a few MHz to as high as 30 MHz, due to the interference within the mirror unit cells.

II. SIMULATION OF PHONON PULSE PROPAGATION

In this section, we show propagation and bouncing of phonon pulses in the cavity-waveguide system (Fig. 3a) can be well simulated by a group of coupled mode equations using input-output formalism. The dynamics captured by the coupled mode equations is a phonon pulse travelling in a waveguide terminated by two cavities with bare mechanical frequency $\omega_{mL,R}$ and waveguide coupling rate $\gamma_{eL,R}$. We approximate $\omega_{mL,R}$ to be the frequency of cavity-dominated modes L_1 and R_1 in the simulation. Since the response time of the optical cavity is much shorter than that of the mechanical cavity, we can exclude the dynamics of optical modes from these equations. Thus, the coupled mode equations can be written as follows,

$$\frac{db_L(t)}{dt} = -(i\omega_{mL} + \frac{\gamma+\gamma_{eL}}{2})b_L(t) - ig_{0L}\alpha_{0L}\alpha^{\star}_{+L}e^{-i\omega_s t}\Theta(t)\Theta(\tau-t) + \sqrt{\gamma_{eL}}b_{\mathrm{in},L}(t), \tag{S-1}$$

$$\frac{db_R(t)}{dt} = -(i\omega_{mR} + \frac{\gamma+\gamma_{eR}}{2})b_R(t) + \sqrt{\gamma_{eR}}b_{\mathrm{in},R}(t), \tag{S-2}$$

$$b_{\mathrm{in},L}(t) = e^{-\alpha l}\big(\sqrt{\gamma_{eR}}b_R(t-t_w) - b_{\mathrm{in},R}(t-t_w)\big), \tag{S-3}$$

$$b_{\mathrm{in},R}(t) = e^{-\alpha l}\big(\sqrt{\gamma_{eL}}b_L(t-t_w) - b_{\mathrm{in},L}(t-t_w)\big), \tag{S-4}$$

where α_{0L} and α_{+L} are the amplitudes of optical pump and its red sideband in the left cavity, τ is the duration of excitation pulse, ω_s is the frequency of pulse, $\Theta(t)$ is the Heaviside step function, γ is the effective decay rate of the excited mechanical mode, $\alpha \approx \gamma/v_g$ is the waveguide loss rate, and $t_w = 1/(2f_{\mathrm{FSR}}) - 1/(\gamma_{eL}+\gamma) - 1/(\gamma_{eR}+\gamma)$ is the single trip time the pulse spent in the waveguide.

From the mechanical spectrum we find $\gamma = 2\pi \times 2.1$ MHz for L_1 mode (the main coherently-driven mode) during the pulse measurement; and by fitting the pulse tails detected in each cavity we find $\gamma_{eL} = 2\pi \times 34.7$ MHz and $\gamma_{eR} = 2\pi \times 25.5$ MHz. Using these parameters, $|b_L|$ and $|b_R|$ can be numerically calculated from the coupled mode equations and the proportional voltage signals are shown in Fig. 3a. The simulated result captures the main features of the measured pulse data. In particular, the pulse splitting observed from cavity R is due to the fact that the pulse frequency is not in resonant with cavity R and thus experiences destructive interference inside this cavity.

The phonon transfer efficiency from cavity L to cavity R is about $e^{-\gamma/(2f_{\mathrm{FSR}})} \approx 67\%$. The phonon transfer efficiency from cavity to waveguide for cavity L and R is $\gamma_{eL(R)}/(\gamma_{eL(R)}+\gamma) \approx 94\%(92\%)$.

We summarize the measured mechanical mode parameters of the device in Fig. 3 in Table I, where g_0 for the

DOI: 10.1038/NPHOTON.2016.107

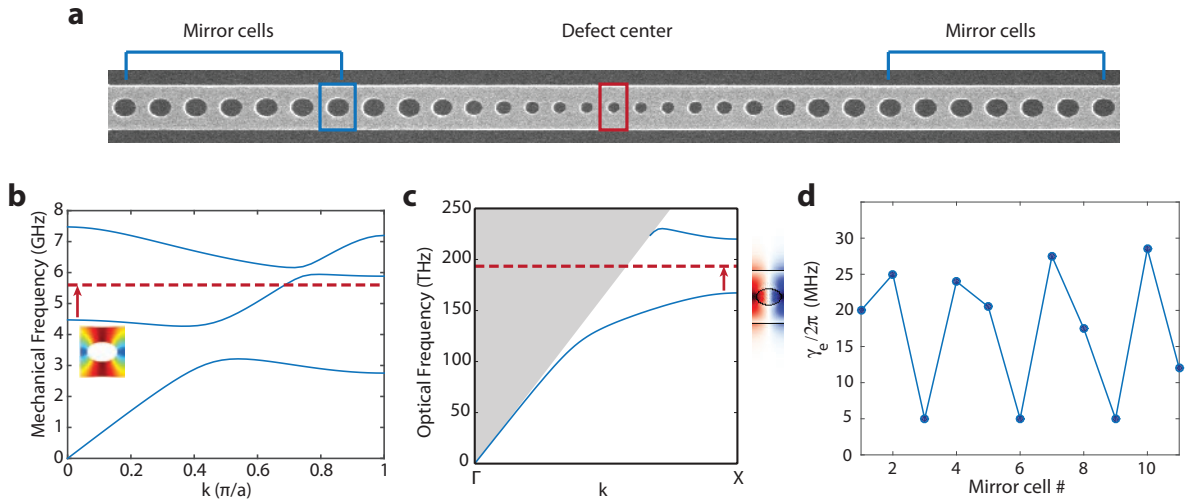

FIG. S-1: **a** SEM image of a typical nanobeam cavity. **b** Mechanical band structure of the mirror cell (blue curves) and mechanical cavity frequency (red dashed line). Inset is the mode profile of second band at Γ point. **c** Optical band structure of the mirror cell (blue curves) and optical cavity frequency (red dashed line). Grey region is light cone. Inset is the mode profile of first band at X point. **d** Oscillation of mechanical cavity and waveguide coupling with variation of number of mirror cells.

TABLE I: Mechanical mode parameters

	$g_0/2\pi$ (MHz)	$\gamma_i/2\pi$ (MHz)	$\gamma_e/2\pi$ (MHz)
L_1	0.85	3.7	34.7
L_2	0.75	3.7	
L_3	0.63	3.9	
R_1	1.39	3.6	25.5

$L_j(R_k)$ modes is with respective to $O_{L(R)}$ optical cavity modes.

III. DERIVATION OF THE MICROWAVE $S-$MATRIX FOR THE OPTOMECHANICAL CAVITY-WAVEGUIDE SYSTEM

Here, we derive the $S-$matrix for a microwave signal traversing the optomechanical cavity-waveguide system. We assume the mechanical amplitude is small such that only the first-order optical sideband needs to be considered. In the next section, we will verify the small mechanical amplitude assumption.

The Hamiltonian of the system under continuous wave operation involves two optical cavity modes $a_{L,R}$ with frequency $\omega_{cL,R}$ parametrically coupled to a common mechanical mode b,

$$\hat{H} = \sum_{k=L,R} \hbar\omega_{ck}\hat{a}_k^\dagger\hat{a}_k + \hbar\omega_m\hat{b}^\dagger\hat{b} + \sum_{k=L,R} \hbar g_{0k}(\hat{b}^\dagger + \hat{b})\hat{a}_k^\dagger\hat{a}_k + \sum_{k=L,R} i\hbar\sqrt{\kappa_{ek}}\alpha_{pk}e^{-i\omega_{pk}t}(\hat{a}_k - \hat{a}_k^\dagger), \tag{S-5}$$

where the last term is the pumps of the two optical cavities. For simplicity we assume the pumping lasers are blue-detuned from the cavity resonances which is true for all of our experiments. Suppose the pumping laser for cavity L is modulated at frequency ω by a microwave signal, then the operators of the system can be decom-

posed into carriers and sidebands,

$$\hat{a}_k = \alpha_{0k} e^{-i\omega_{pk}t} + \alpha_{+k} e^{-i(\omega_{pk}-\omega)t}, \quad \hat{b} = \beta_- e^{-i\omega t}, \tag{S-6}$$

where we only keep the red sideband of the pumping lasers because of rotating wave approximation, given the sideband resolved condition $\omega_m \gg \kappa_k$ of our device. Suppose the pumps are strong enough such that the carrier operators can be treated as static variables, then the equations of motion of the system can be derived after substituting Eq. S-6 into Eq. S-5,

$$i\omega\alpha_{+k} = (i\Delta_k - \frac{\kappa_k}{2})\alpha_{+k} - ig_{0k}\alpha_{0k}\beta_-^\star - \sqrt{\kappa_{ek}}\alpha_{\mathrm{in,k}}, \tag{S-7}$$

$$-i\omega\beta_- = -(i\omega_m + \frac{\gamma_i}{2})\beta_- - \sum_k ig_{0k}\alpha_{0k}\alpha_{+k}^\star, \tag{S-8}$$

where $\Delta_k = \omega_{pk} - \omega_{ck} \approx \omega_m$. Solving Eq. S-7 and Eq. S-8 in the frequency range $|\omega - \omega_m| \ll \kappa_k$, we obtain

$$\beta_- = \frac{ig_{0L}\sqrt{\kappa_{eL}}\frac{2}{\kappa_L}\alpha_{0L}}{i(\omega_m - \omega) + \frac{\gamma_i}{2} - \sum_k \frac{2g_{0k}^2|\alpha_{0k}|^2}{\kappa_k}}\alpha_{\mathrm{in},L}^\star, \tag{S-9}$$

$$\begin{aligned}\alpha_{\mathrm{out},R} &= -\sqrt{\kappa_{eR}}\alpha_{+R} \\ &= -\frac{4g_{0L}g_{0R}\sqrt{\kappa_{eL}\kappa_{eR}}/(\kappa_L\kappa_R)\alpha_{0L}^\star\alpha_{0R}}{i(\omega_m - \omega) + \frac{\gamma_i}{2} - \sum_k \frac{2g_{0k}^2|\alpha_{0k}|^2}{\kappa_k}}\alpha_{\mathrm{in},L}.\end{aligned} \tag{S-10}$$

From Eq. S-10, peak optical gain at $\omega = \omega_m$ is

$$G_{\max} = \frac{|\alpha_{\mathrm{out},R}|^2}{|\alpha_{\mathrm{in},L}|^2} = \frac{4C_LC_R}{(1 - C_L - C_R)^2}, \tag{S-11}$$

where $C_{L(R)} = |\gamma_{\mathrm{OM},L(R)}|/\gamma_i$ is the coorperativity of mechanical mode b with optical modes $a_{L(R)}$.

Using the result of Eq. S-10, the microwave signal transfer $S-$matrix can be derived

$$\begin{aligned}&S_{RL} \\ &\equiv \frac{V_{\mathrm{NA,in}}}{V_{\mathrm{NA,out}}} \\ &= \frac{\eta_{oL}\eta_{oR}G_eG_{\mathrm{EDFA}}(i\hbar\omega_{cR}\omega_m/\sqrt{\kappa_{eR}})\alpha_{\mathrm{out},R}\alpha_{0R}^\star}{(2V_\pi/\pi)\left(\alpha_{\mathrm{in},L}/(i\omega_m\alpha_{0L}/\sqrt{\kappa_{eL}})\right)} \\ &= \frac{\eta_{oL}\eta_{oR}G_eG_{\mathrm{EDFA}}}{2V_\pi/\pi}\frac{4g_{0L}g_{0R}\hbar\omega_{cR}\omega_m^2/(\kappa_L\kappa_R)|\alpha_{0L}|^2|\alpha_{0R}|^2}{i(\omega_m - \omega) + \frac{\gamma_i}{2} - \sum_k \frac{2g_{0k}^2|\alpha_{0k}|^2}{\kappa_k}}\end{aligned} \tag{S-12}$$

where $V_{\mathrm{NA,out}}$ and $V_{\mathrm{NA,in}}$ are the output and detected electrical voltage of the network analyzer respectively, $\eta_{oL,R}$ is the optical loss of the input and output ports of the device and fiber respectively, G_{EDFA} and G_e are the gain coefficients of EDFA and photodetector respectively, and V_π is the voltage required to produce a phase shift of π of the electro-optic modulator.

IV. ANALYSIS OF LINEAR OPERATION AND NOISE CHARACTERISTICS OF THE OPTOMECHANICAL MICROWAVE FILTER/DELAY LINE

In this section, we examine the assumption of weak mechanical amplitude under strong optical pump and analyze the optomechanical microwave filter/delay line performance in terms of linearity and noise characteristics. We find that thermo-optic effect constrains the mechanical amplitude due to saturation of the optomechanical gain. This effect sets the linear operation range and the suppression of the mechanical thermal noise.

The thermo-optic effect induced optical cavity frequency shift can be described by the following equations [1]

$$\delta\omega_c = -\omega_c n_{\mathrm{Si}}(T_0)\frac{dn_{\mathrm{Si}}(T_0)}{dT}A\delta T, \tag{S-13}$$

$$\delta T = \frac{r\varsigma c^2}{n_{\mathrm{Si}}(T_0)^2 V_{\mathrm{TPA}}}n_c^2, \tag{S-14}$$

where n_c is cavity photon number, n_{Si}, r, and ς is the refractive index, thermal resistance, and two-photon absorption coefficient of silicon respectively, c is the speed of light, V_{TPA} is the cavity volume for two-photon absorption, and A is a perturbation theory coefficient $A = \frac{\int_{\mathrm{Si}}|\mathbf{E}(\mathbf{r})|^2 d\mathbf{r}}{\int n_{\mathrm{Si}}(T_0)^2|\mathbf{E}(\mathbf{r})|^2 d\mathbf{r}}$. Substituting Eq. S-14 into Eq. S-13, and using the parameters of silicon given in Ref. [1], along with $A \approx 7.5 \times 10^{-2}$, $V_{\mathrm{TPA}} \approx (\lambda/n_{\mathrm{Si}}(T_0))^3$, we have

$$\delta\omega_c = \xi n_c^2, \quad \xi \approx -33.9 \text{ Hz}. \tag{S-15}$$

We proceed to include the term of thermo-optic effect (Eq. S-15) to the equations of motion (Eqs. S-7 and S-8), which are then modified to be

$$i\omega\bar{\alpha}_+ = \Big(i\big(\Delta + \xi(|\alpha_0|^2 + |\bar{\alpha}_+|^2)^2\big) - \frac{\kappa}{2}\Big)\bar{\alpha}_+ - ig_0\alpha_0\bar{\beta}_-^\star, \tag{S-16}$$

$$-i\omega\bar{\beta}_- = -(i\omega_m + \frac{\gamma_i}{2})\bar{\beta}_- - ig_0\alpha_0\bar{\alpha}_+^\star - \sqrt{\gamma_i}\beta_{\mathrm{in}}, \quad \beta_{\mathrm{in}} = \sqrt{\gamma_i n_{\mathrm{th}}}/2, \tag{S-17}$$

where we have denoted $\bar{\alpha}_+$ and $\bar{\beta}_-$ as the static value of the corresponding operators without input optical side-

DOI: 10.1038/NPHOTON.2016.107

band signal and we have included the mechanical thermal noise input. Also, we specifically consider the operation with the R_1 mode, and thus ignore optical cavity L which has much weaker coupling with R_1 compared to optical cavity R. Eqs. S-16 and S-17 can only be solved numerically for a generic pump condition. To reveal the thermo-optic effect on the mechanical amplitude, we consider a special pump condition corresponding to the original threshold of mechanical self-oscillation, i.e. $4g_0^2|\alpha_0|^2/(\kappa\gamma_i) = 1$. In this case, we can analytically solve for the down-converted photon number and mechanical amplitude at $\omega = \omega_m$ from Eqs. S-16 and S-17, assuming $\Delta = \omega_m$ and $|\bar{\alpha}_+| \gg |\alpha_0|$,

$$|\bar{\alpha}_+|^2 = (\frac{\kappa\gamma_i n_{\rm th}}{4\xi^2})^{1/5}, \tag{S-18}$$

$$|\bar{\beta}_-|^2 = \frac{\kappa}{\gamma_i}(\frac{\kappa\gamma_i n_{\rm th}}{4\xi^2})^{1/5} + n_{\rm th}. \tag{S-19}$$

For $\kappa = 2\pi\times 0.8$ GHz, $\gamma_i = 2\pi\times 3.6$ MHz, $g_0 = 2\pi\times 1.39$ MHz, $n_{\rm th} = \frac{k_B T_0}{\hbar\omega_m} \approx 1000$, we have $|\bar{\alpha}_+|^2 \approx 1900$, $|\alpha_0|^2 \approx 380$, and $|\bar{\beta}_-|^2 \approx 3.7\times 10^5$. It is the optical resonance shift induced by thermo-optic effect that saturates optomechanical gain and prevents runaway of the mechanical amplitude at the threshold.

Now we can estimate whether the mechanical amplitude is large enough to induce nonlinearity through excitation of higher order optical sidebands. The nonlinearity arises due to pump saturation and occurs when the amplitude of the first order optical sideband significantly deviates from being linearly proportional to the mechanical amplitude, i.e. approximation $J_1(z) \approx \frac{z}{2}$ breaks down [2], where $z = g_0\sqrt{4|\bar{\beta}_-|^2+2}/\omega_m$ is the normalized mechanical amplitude. For $|\bar{\beta}_-|^2 \approx 3.7\times 10^5$ calculated above, the deviation is only about 1%. In the experiment, we find for the largest pump power $P_{pL,R} \approx 0.2$ mW, $|\bar{\beta}_-|^2 \approx 2.0\times 10^5$, which gives $z = 0.18$ and a linear deviation of 0.4%. As a result, scattering into higher order optical sidebands does not need to be included in Eq. (S-16) and (S-17).

Next, we consider the response of the mechanical oscillator to a small input optical sideband signal by perturbative expansion of Eqs. S-16 and S-17. In this case the coherent mechanical amplitude of Eq. S-9 is modified to be

$$\beta_- = \frac{ig_{0L}\sqrt{\kappa_{eL}}\frac{2}{\kappa_L}\alpha_{0L}}{i(\omega_m-\omega)+\frac{\gamma_i}{2}-\sum_k \frac{2g_{0k}^2|\alpha_{0k}|^2}{-2i\delta_k+\kappa_k}}\alpha^\star_{{\rm in},L}, \tag{S-20}$$

where $\delta_k = \xi(|\alpha_{0k}|^2+|\bar{\alpha}_{+k}|^2)^2$ is the thermo-optic-effect induced optical frequency shift. Eqs. S-10 and S-12 can be modified correspondingly. According to Eq. S-20, the effective mechanical loss rate is $\gamma_{\rm eff} = \gamma_i - \sum_k \frac{4g_{0k}^2|\alpha_{0k}|^2}{\kappa_k} + \sum_k \frac{4g_{0k}^2|\alpha_{0k}|^2}{\kappa_k}(\frac{\delta_k}{\kappa_k/2})^2$. The deviation from a linear response can be caused by the additional cavity photons from the input signal, and is characterized by the ratio $r = |\alpha_{+k}|^2/|\bar{\alpha}_{+k}|^2$ (in our device the contribution is mainly from α_{+R}). At the theoretical self-oscillation threshold, we find the 1 dB compression point of the $S-$matrix to be equal to a microwave power of -19 dBm (assuming $|\alpha_{0L}|^2 = |\alpha_{0R}|^2$). In the experiment, we find for the largest optical pump power $P_{pL,R} = 0.2$ mW (which is slightly above the self-oscillation threshold), the 1 dB compression point occurs at a microwave signal power of -15 dBm. For reversed operation (cavity R as input), the 1 dB compression point is reduced by a factor of $\gamma_{{\rm OM},L}/\gamma_{{\rm OM},R}$ (assuming $|\alpha_{0L}|^2 = |\alpha_{0R}|^2$).

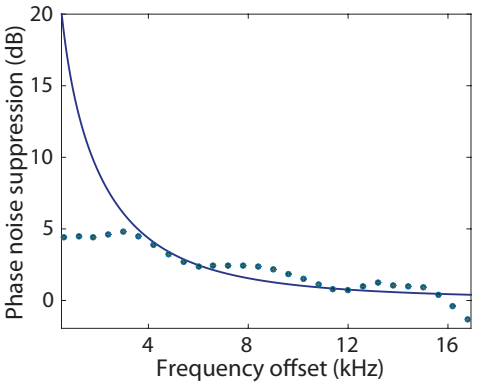

FIG. S-2: Phase noise suppression ratio between microwave signal power of -15 dBm and -30 dBm at largest optical pump level. Solid line is theoretical value calculated using Eq. S-23 and dots are experimental data.

We now analyze the noise characteristics of the optomechanical cavity-waveguide system. The dominant form of noise is from thermally excited phonons in the system. From the thermally-added mechanical noise refered to the input signal $(\kappa_e/\kappa)^{-1}\gamma_i n_{\rm th}/|\gamma_{\rm OM}|$ [3], we define the noise-equivalent optical signal power

$$P_{\rm NE} = \frac{\kappa}{\kappa_e}\hbar\omega_c\frac{\gamma_i n_b}{\gamma_{\rm OM}}2\pi B, \tag{S-21}$$

where B is the bandwidth of the coherent signal and all the quantities are referred to the input cavity. Then the noise-equivalent microwave signal power is

$$V_{NE}^2 = \frac{4}{\pi^2}\frac{P_{\rm NE}}{P_p}V_\pi^2. \tag{S-22}$$

We find that for the largest pump power when operating at R_1 resonance, if the input port is cavity L, the noise equivalent microwave power is -30 dBm; if the input port is cavity R, the noise equivalent microwave power reduces to -70 dBm because of the significantly enhanced $\gamma_{\rm OM}$ of cavity R with R_1 mode.

For a self-oscillating mechanical oscillator, the intrinsic oscillator noise can be suppressed by the injection of an external coherent signal [4]. The suppressed phase noise

(ignoring input signal noise) can be modeled by [5]

$$\tilde{S}_{\phi\phi}(\omega-\omega_m)=\frac{1}{1+(\frac{\gamma_{\rm eff}}{\omega-\omega_m})^2\rho^2}S_{\phi\phi}(\omega-\omega_m), \quad \text{(S-23)}$$

where $S_{\phi\phi}(\omega)$ is the intrinsic phase noise spectral density without injection and $\rho=|\beta_-|/|\bar{\beta}_-|$ is the ratio between injected mechanical amplitude and free-running amplitude. Experimentally, we infer the phase noise from the measured noise power spectral density using the definition $S_{\phi\phi}(\omega)=S_{bb}(\omega)-\int S_{bb}(\omega)d\omega$. At the largest optical pump level, the phase noise suppression ratio between the microwave signal power -15 dBm (1 dB $S-$matrix compression point) and -30 dBm (noise equivalent power) is shown in Fig. S-2. The model of Eq. S-23 explains well the measured noise suppression level in the offset frequency $(\omega-\omega_m)$ range between $\gamma_{\rm eff}/4$ and $3\gamma_{\rm eff}/4$ ($\gamma_{\rm eff}=2\pi\times 17$ kHz).

V. WAVEGUIDE-MEDIATED CAVITY COUPLING

A. Analytical derivation

When $\gamma_{eL,R}/2\pi \ll f_{\rm FSR}$, and all the waveguide modes are outside of the line width of the cavities, two mechanical cavities can acquire a waveguide mediated coupling. The generic Hamiltonian describing this case is

$$\hat{H}=\hbar\omega_{mL}\hat{b}_L^\dagger\hat{b}_L+\hbar\omega_{mR}\hat{b}_R^\dagger\hat{b}_R+\sum_k\hbar\omega_k\hat{b}_k^\dagger\hat{b}_k+\sum_k\hbar(g_{Lk}\hat{b}_L^\dagger\hat{b}_k+g_{Lk}^\star\hat{b}_L\hat{b}_k^\dagger)+\sum_k\hbar(g_{Rk}\hat{b}_R^\dagger\hat{b}_k+g_{Rk}^\star\hat{b}_R\hat{b}_k^\dagger), \quad \text{(S-24)}$$

where $b_k^\dagger(b_k)$ is the creation(annihilation) operator of the $k-$th waveguide mode, $g_{Lk}=\sqrt{2\gamma_{eL}f_{\rm FSR}}$ and $g_{Rk}=(-)^k\sqrt{2\gamma_{eR}f_{\rm FSR}}$ are the coupling coefficients of the left and right mechanical cacity modes with the $k-$th waveguide mode, and the summation is over all waveguide modes. Note the relative sign between g_{Lk} and g_{Rk} comes from the symmetry of waveguide modes with respect to the center of the two cavities.

In the degenerate cavity case, i.e. $\omega_{mL}=\omega_{mR}$, we can calculate the coupling V between the two cavities mediated by the waveguide modes using second order perturbation theory as follows,

$$\begin{aligned}\frac{V}{2\pi} &= \sum_{k=-\infty}^{\infty}\frac{\frac{g_{Lk}}{2\pi}\frac{g_{Rk}}{2\pi}}{\delta-kf_{\rm FSR}} \quad \text{(S-25)}\\ &= \frac{\sqrt{\gamma_{eL}\gamma_{eR}}}{2\pi}\sum_{k=-\infty}^{\infty}\frac{(-)^k}{\frac{\delta}{f_{\rm FSR}}\pi-k\pi}\\ &= \frac{\sqrt{\gamma_{eL}\gamma_{eR}}}{2\pi}\frac{1}{\sin\frac{\delta}{f_{\rm FSR}}\pi},\end{aligned}$$

where δ is the frequency difference between the degenerate cavity modes and their nearest waveguide mode. For the perturbation theory to be valid, we require

$$|g_{L,Rk}|/2\pi=\sqrt{2\gamma_{eL,R}f_{\rm FSR}}/2\pi\ll\delta. \quad \text{(S-26)}$$

We consider two special cases. First, when $\delta=f_{\rm FSR}/2$, i.e. the two cavity modes are in the center of two nearest waveguide modes, then $V=\sqrt{\gamma_{eL}\gamma_{eR}}$. In the other limit when $\delta\ll f_{\rm FSR}$, then $V\approx\sqrt{\gamma_{eL}\gamma_{eR}}\frac{f_{\rm FSR}}{\pi\delta}$. One can prove in this case, $V\ll\sqrt{2\gamma_{eL,R}f_{\rm FSR}}=|g_{L,Rk}|$, by taking into account of the condition of Eq. S-26. Different from the previous case, here the contribution to the coupling can be almost exclusively attributed the nearest waveguide mode ($k=0$).

B. Measurement modeling

We model how to estimate the phonon waveguide mediated coupling between two optomechanical cavities. In the device for demonstrating waveguide-mediated cavity coupling, we used a phonon waveguide without air holes. The band structure of the waveguide is shown in Fig. S-3a. Such a waveguide provides large phonon group velocity and thus large free spectral range in order to isolate cavity modes from waveguide modes.

In the sample device shown in Fig. 4 of the main text, virtual phonons in waveguide mixes the mechanical cavity modes M_L and M_R of cavity L and R into hybridized modes M_+ and M_-. The coupling strength can be inferred by measuring the optomechanical coupling of hybridized modes M_+ and M_- with the two optical modes O_L and O_R based on the following model. M_+ and M_- can be expressed as linear superposition of M_L and M_R, assuming ignorable energy distribution in the waveguide (as $M_{+,-}$ are well separated from waveguide modes),

$$M_+=\alpha_1M_L+\alpha_2M_R, \quad \text{(S-27)}$$
$$M_-=\beta_1M_L+\beta_2M_R. \quad \text{(S-28)}$$

The superposition coefficients α_i and β_i satisfy the following relation

$$|\frac{\beta_1}{\alpha_1}|=|\frac{\alpha_2}{\beta_2}|=\frac{2|V|}{\Delta_{LR}+\Delta_{+-}}, \quad \text{(S-29)}$$

DOI: 10.1038/NPHOTON.2016.107

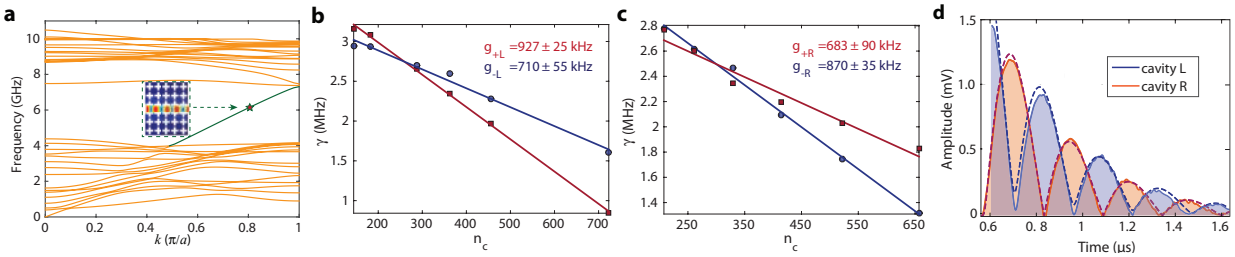

FIG. S-3: **a** Band structure of shielded phonon waveguide without air holes. Inset is the modal profile with $k = 0.8\pi/a$. **b,c** Characterization of optomechanical coupling between hybridized mechanical modes M_+ and M_- with the optical modes of cavity L (**b**) and R (**c**). $\gamma = \gamma_i + \gamma_{\rm OM}$ is effective mechanical decay rate and n_c is the cavity photon number. **d** Simulated phonon evolution using coupled mode equations (dashed lines). Solid lines are experiment data.

where V is the waveguide mediated coupling between M_L and M_R, Δ_{LR} is the fabrication induced frequency difference between M_L and M_R, and $\Delta_{+-} = \sqrt{\Delta_{LR}^2 + 4V^2}$ is the frequency difference between the hybridized modes M_+ and M_-. On the other hand, the ratio of the superposition coefficients is directly related to the measurable optomechanical coupling

$$\frac{g_{+L}}{g_{-L}} = |\frac{\alpha_1}{\beta_1}|, \quad \frac{g_{+R}}{g_{-R}} = |\frac{\alpha_2}{\beta_2}|, \tag{S-30}$$

where, for example, g_{+L} stands for the vacuum optomechanical coupling between mechanical mode M_+ and optical mode O_L.

We inferred the optomechanical couplings by measuring the pump dependent effective mechanical damping rate of $M_{+,-}$ (Fig. S-3b,c) using the relation $\gamma = \gamma_i - g^2 n_c \frac{\kappa}{(\Delta-\omega_m)^2+\kappa^2/4}$, and obtained

$$g_{+L} = 927 \pm 25 \text{ kHz}, \quad g_{-L} = 710 \pm 55 \text{ kHz} \tag{S-31}$$
$$g_{+R} = 683 \pm 90 \text{ kHz}, \quad g_{-R} = 870 \pm 35 \text{ kHz} \tag{S-32}$$

As a result, the ratio of superposition coefficients is

$$|\frac{\alpha_1}{\beta_1}| = 1.30 \pm 0.14, \quad |\frac{\alpha_2}{\beta_2}| = 0.79 \pm 0.14. \tag{S-33}$$

Along with $\Delta_{+-}/2\pi = 4.0$ MHz as read from the spectrum, we find, according to Eq. S-29,

$$|V|/2\pi = 1.94 \pm 0.06 \text{ MHz}, \ \Delta_{LR}/2\pi = 0.98 \pm 0.48 \text{ MHz}. \tag{S-34}$$

To compare with the analytical formula of V (Eq. S-25), in this device, we have $f_{\rm FSR} = 54$ MHz and $\delta = 17$ MHz. And using the measured $V/2\pi = 1.94$ MHz, we find $\sqrt{\gamma_{eL}\gamma_{eR}}/2\pi = 1.62$ MHz.

C. Simulation of Rabi oscillation

With the mode parameters obtained from above, we can simulate the Rabi oscillation using coupled mode equations. In contrast to the coupled mode equations used to simulate pulse propagation through waveguide (Eqs. S-1-S-4), the new set of equations describe only two-mode coupling and do not contain the process of propagation in the waveguide, which read:

$$\frac{db_L(t)}{dt} = -(i\omega_{mL} + \frac{\gamma_L}{2})b_L(t) + iVb_R(t) - ig_{0L}\alpha_{0L}\alpha_{+L}^{\star}e^{-i\omega_s t}\Theta(t)\Theta(\tau - t), \tag{S-35}$$

$$\frac{db_R(t)}{dt} = -(i\omega_{mR} + \frac{\gamma_R}{2})b_R(t) + iVb_L(t). \tag{S-36}$$

Using $\gamma_L = \gamma_R = 2\pi\times 1$ MHz, $V/2\pi = 2$ MHz, $\Delta_{LR}/2\pi = 0.5$ MHz, we calculated the phonon population evolution in the two cavities, which is shown in Fig. S-3d as the dashed curves.

VI. OPTICAL NON-RECIPROCITY BASED ON DISTANTLY-COUPLED OPTOMECHANICAL CAVITIES

We provide theoretical analysis of achieving optical non-reciprocity in the distantly-coupled optomechanical

cavities, and show its viability based on the typical parameters of our fabricated devices. In this case, the waveguide connecting the two cavities should support both guided mechanical and optical modes, and the two optomechanical cavities are designed to be identical. As already been demonstrated in our experiment and in Ref. [6] respectively, such a waveguide can mediate a tight-binding type coupling for the mechanical and optical cavity modes. The Hamiltonian of the system can thus be written as follows,

$$\begin{aligned}\hat{H} &= \sum_{k=L,R}\hbar\omega_{ck}\hat{a}_k^\dagger\hat{a}_k + J(a_L^\dagger a_R + a_L a_R^\dagger) + \sum_{k=L,R}\hbar\omega_{mk}\hat{b}_k^\dagger\hat{b}_k + V(b_L^\dagger b_R + b_L b_R^\dagger) \\ &+ \sum_{k=L,R}\hbar g_k(\hat{b}_k^\dagger + \hat{b}_k)\hat{a}_k^\dagger\hat{a}_k + \sum_{k=L,R} i\hbar\sqrt{\kappa_{ek}}\alpha_{pk}e^{-i\omega_p t - i\varphi_k}(\hat{a}_k - \hat{a}_k^\dagger),\end{aligned} \tag{S-37}$$

where J and V are the waveguide mediated optical and mechanical coupling strength, and the last two terms are the optical pumps in the two cavities which have a same frequency and correlated phases.

The optical non-reciprocity arisen from this system can be intuitively understood from a schematic shown in Fig. S-4a. The input optical signal undergoes a Mach-Zehnder type of interference through the system: one path is the direct photon hopping and the other path is through radiation-pressure interaction induced transition to phonon and phonon hopping. The phase of the latter path involves the phase difference of the two pumps, which is $\varphi_L - \varphi_R$ for one direction and $\varphi_R - \varphi_L$ for the reversal direction. Such a non-reciprocal phase resembles an effective magnetic flux for photons, resulting in the non-reciprocal transmission [7].

We first consider the case when both cavities are being pumped with blue detuned lasers ($\omega_p - \omega_{ck} = \omega_{mk}$). The equations of motion of the system, in terms of red optical sidebands of the pumps, can be derived from the Hamiltonian of Eq. S-37 using rotating wave approximation, given sideband resolved condition $\omega_{mk} \gg \kappa_k$,

$$\frac{da_L}{dt} = (i\delta_L - \frac{\kappa_L}{2})a_L - iJa_R - ig_L\alpha_L e^{i\phi_L}b_L^\star - \sqrt{\kappa_{eL}}a_{L,\mathrm{in}}, \tag{S-38}$$

$$\frac{da_R}{dt} = (i\delta_R - \frac{\kappa_R}{2})a_R - iJa_L - ig_R\alpha_R e^{i\phi_R}b_R^\star - \sqrt{\kappa_{eR}}a_{R,\mathrm{in}}, \tag{S-39}$$

$$\frac{db_L}{dt} = -(i\omega_{mL} + \frac{\gamma_i}{2})b_L - iVb_R - ig_L\alpha_L e^{i\phi_L}a_L^\star, \tag{S-40}$$

$$\frac{db_R}{dt} = -(i\omega_{mR} + \frac{\gamma_i}{2})b_R - iVb_L - ig_R\alpha_R e^{i\phi_R}a_R^\star, \tag{S-41}$$

where $\delta_k = \omega_p - \omega_{ck}$ and $\alpha_k e^{i\phi_k}$ is the steady state amplitude of the local optical cavity mode, which is related to the pumping amplitudes as follows

$$\alpha_{L(R)}e^{i\phi_{L(R)}} = \frac{(i\delta_{R(L)} - \kappa_{R(L)}/2)\sqrt{\kappa_{eL(R)}}\alpha_{pL(R)}e^{-i\varphi_{L(R)}} + iJ\sqrt{\kappa_{eR(L)}}\alpha_{pR(L)}e^{-i\varphi_{R(L)}}}{(i\delta_L - \kappa_L/2)(i\delta_R - \kappa_R/2) + J^2}. \tag{S-42}$$

We find the steady state amplitude is approximately $\sqrt{\kappa_{ek}}\alpha_{pk}e^{-i\varphi_k}/i\delta_k$ under the condition $\delta_k \approx \omega_{mk} \gg \kappa_k, J$, which means each cavity is effectively only driven by its own optical pump. This can be intuitively understood by the fact that even and odd hybridized optical cavity modes are driven equally (as $\delta_k \gg J$) and thus the amplitude of one local cavity mode is cancelled out and effectively not being driven. Thus, each cavity-enhanced optomechnical coupling can be independently controlled by the pump.

DOI: 10.1038/NPHOTON.2016.107

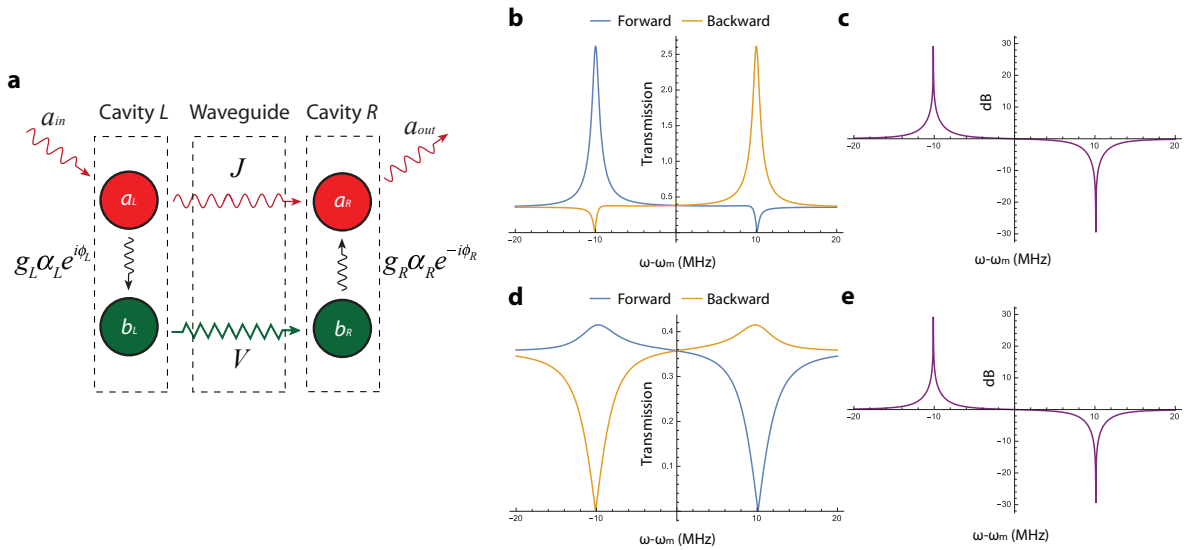

FIG. S-4: **a** Schematic of the optical non-reciprocity in distantly-coupled optomechanical cavities stemmed from the non-reciprocal optical pump phases and interference between photonic and phononic transmission paths. **b-e** Transmission coefficient **b**(**d**) and isolation ratio **c**(**e**) for blue(red) detuned optical pumps with practical device parameters $\gamma_i = 2\pi \times 3$ MHz, $g_{L,R} = 2\pi \times 0.8$ MHz, cavity photon number $n_{cL,R} = 2000$, $\kappa_{L,R} = 2\pi \times 2$ GHz, $\kappa_{eL,R} = 2\pi \times 1$ GHz, $\phi_L - \phi_R = \frac{\pi}{2}$, $J = 2\pi \times 422$ MHz, and $V = 2\pi \times 10$ MHz.

After solving the equations of motion, we calculate the ratio between right transmission coefficient T_R and left transmission coefficient T_L of the optical signal and find

$$\frac{T_R}{T_L} = \frac{J - \frac{V g_L g_R \alpha_L \alpha_R}{(i(\omega-\omega_{mL})+\frac{\gamma_i}{2})(i(\omega-\omega_{mR})+\frac{\gamma_i}{2})+V^2} e^{i(\phi_L-\phi_R)}}{J - \frac{V g_L g_R \alpha_L \alpha_R}{(i(\omega-\omega_{mL})+\frac{\gamma_i}{2})(i(\omega-\omega_{mR})+\frac{\gamma_i}{2})+V^2} e^{-i(\phi_L-\phi_R)}}. \tag{S-43}$$

Interestingly, this ratio is not explicitly dependent on δ_k and κ_k as an intrinsic property of the device. At the poles $\omega = (\omega_{mL} + \omega_{mR} \pm \sqrt{(\omega_{mL} - \omega_{mR})^2 + 4V^2})/2$, i.e. frequency of the hybridized mechanical modes, and assuming $V \gg \gamma_i$, we have

$$\frac{T_R}{T_L} = \frac{J \pm i\frac{V g_L g_R \alpha_L \alpha_R}{\gamma_i \sqrt{V^2+(\omega_{mL}-\omega_{mR})^2/4}} e^{i(\phi_L-\phi_R)}}{J \mp i\frac{V g_L g_R \alpha_L \alpha_R}{\gamma_i \sqrt{V^2+(\omega_{mL}-\omega_{mR})^2/4}} e^{-i(\phi_L-\phi_R)}}. \tag{S-44}$$

Thus perfect non-reciprocity, i.e. one direction has vanishing transmission while the other direction has maximal transmission, can be achieved by satisfying the following condition

$$\phi_L - \phi_R = \pm\frac{\pi}{2}, \quad J = \frac{V g_L g_R \alpha_L \alpha_R}{\gamma_i \sqrt{V^2 + (\omega_{mL} - \omega_{mR})^2/4}}. \tag{S-45}$$

Under this condition, the transmission coefficient for the through direction is (for simplicity assuming $\omega_{mL} = \omega_{mR}$)

$$T_{\neq 0} = \sqrt{\kappa_{eL}\kappa_{eR}} \frac{2\frac{g_L g_R \alpha_L \alpha_R}{\gamma_i}}{(\frac{\kappa_L}{2} - \frac{g_L g_R \alpha_L \alpha_R}{\gamma_i})(\frac{\kappa_R}{2} - \frac{g_L g_R \alpha_L \alpha_R}{\gamma_i})}. \tag{S-46}$$

Similar results can be derived for the case of red detuned pumps, and we find the perfect non-reciprocity condition (Eq. S-45) remains the same; while the transmission coefficient for the through direction at poles is given by

$$T_{\neq 0} = \sqrt{\kappa_{eL}\kappa_{eR}} \frac{2\frac{g_L g_R \alpha_L \alpha_R}{\gamma_i}}{(\frac{\kappa_L}{2} + \frac{g_L g_R \alpha_L \alpha_R}{\gamma_i})(\frac{\kappa_R}{2} + \frac{g_L g_R \alpha_L \alpha_R}{\gamma_i})}. \tag{S-47}$$

We note, in general, an amplified transmission in blue detuned case and an attenuated transmission in red detuned case for the through direction at poles. One can prove from Eq. S-47 that in the red detuned case, $T_{\neq 0} \leq \sqrt{\kappa_{eL}\kappa_{eR}/(\kappa_L\kappa_R)} < 1$ and equality is achieved when $\kappa_k/2 = \frac{g_L g_R \alpha_L \alpha_R}{\gamma_i}$. Comparing to Eq. S-45, the maximal transmission efficiency is achieved when loss rate $\kappa_k/2$ and coupling rate J is matched at the two cavities (note we used $\omega_{mL} = \omega_{mR}$ for Eqs. S-46 and S-47).

Based on our fabricated devices, realizing the conditions for perfect non-reciprocity (Eq. S-45) is quite promising. For a typical device with $\gamma_i = 2\pi \times 3$ MHz, $g_L = g_R = 2\pi \times 0.8$ MHz, maximal available cavity photon number $n_{cL} = n_{cR} = 2000$, and assuming

$\omega_{mL} = \omega_{mR}$, Eq. S-45 determines $J_{\max} = 422$ MHz. Thus, as long as $J \leq J_{\max}$ in this device, perfect non-reciprocity condition can always be achieved by tuning the pump power and phase. We have numerically simulated waveguide (without acoustic shielding) mediated optical coupling between two optomechanical cavities to be 500 MHz and less. Thus it is indeed viable to demonstrate optical non-reciprocity in our devices. Using these parameters along with $\delta_k = \omega_{mk}$, $\kappa_k = 2\pi \times 2$ GHz, $\kappa_{ek} = 2\pi \times 1$ GHz and $\phi_L - \phi_R = \frac{\pi}{2}$, $J = 2\pi \times 422$ MHz, $V = 2\pi \times 10$ MHz, we plotted the transmission coefficients and isolation ratio as calculated from Eqs. S-38–S-41 for the blue-detuned pump In Fig. S-4b,c and red-detuned pump In Fig. S-4d,e, respectively.

[1] T. Uesugi, B.-S. Song, T. Asano, and S. Noda, "Investigation of optical nonlinearities in an ultra-high-q si nanocavity in a two-dimensional photonic crystal slab," *Opt. Express*, vol. 14, pp. 377–386, 2006.

[2] F. Marquardt, J. G. E. Harris, and S. M. Girvin, "Dynamical multistability induced by radiation pressure in high-finesse micromechanical optical cavities," *Phys. Rev. Lett.*, vol. 96, p. 103901, 2006.

[3] J. T. Hill, A. H. Safavi-Naeini, J. Chan, and O. Painter, "Coherent optical wavelength conversion via cavity-optomechanics," *Nature Communications*, vol. 3, p. 1196, 2012.

[4] M. Hossein-Zadeh and K. Vahala, "Observation of injection locking in an optomechanical rf oscillator," *Appl. Phys. Lett.*, vol. 93, p. 191115, 2008.

[5] H.-C. Chang, X. Cao, U. K. M. M. J. Vaughan, and R. A. York, "Phase noise in externally injection-locked oscillator arrays," *IEEE Transactions on Microwave Theory and Techniques*, vol. 45, pp. 2035–2042, 2007.

[6] Y. Sato, Y. Tanaka, J. Upham, Y. Takahashi, T. Asano, and S. Noda, "Strong coupling between distant photonic nanocavities and its dynamic control," *Nat. Photons.*, vol. 6, pp. 56–61, 2012.

[7] K. Fang, Z. Yu, and S. Fan, "Photonic aharonov-bohm effect based on dynamic modulation," *Phys. Rev. Lett.*, vol. 108, p. 153901, 2012.